3D Printing of Customized Drug Delivery Systems with Controlled Architecture via Reversible Addition-Fragmentation Chain Transfer Polymerization

Ali Bagheri,* Mitra Asadi-Eydivand, Adam A. Rosser, Christopher M. Fellows, and Trevor C. Brown

3D printing via reversible addition-fragmentation chain transfer (RAFT) polymerization has been recently developed to expand the scope of 3D printing technologies. A potentially high-impact but relatively unexplored opportunity that can be provided by RAFT-mediated 3D printing is a pathway toward personalized medicine through manufacturing bespoke drug delivery systems (DDSs). Herein, 3D printing of drug-eluting systems with precise geometry, size, drug dosage, and release duration/profiles is reported. This is achieved through engineering a range of 3D models with precise interconnected channel-pore structure and geometric proportions in architectural patterns. Notably, the application of the RAFT process is crucial in manufacturing materials with highly resolved macroscale features by confining curing to exposure precincts. This approach also allows spatiotemporal control of the drug loading and compositions within different layers of the scaffolds. The ratio between the polyethylene glycol units and the acrylate units in the crosslinkers is found to be a critical factor, with a higher ratio increasing swelling capacity, and thus enhancing the drug release profile, from the drug-eluting systems. This proof-of-concept research demonstrates that RAFT-mediated 3D printing enables the production of personalized drug delivery materials, providing a pathway to replace the "one-size-fits-all" approach in traditional health care.

1. Introduction

3D printing provides a programmable pathway for the fabrication of customized and on-demand materials.[1] The scientific and technological impacts of 3D printing in various sectors, including engineering, automotive, and health care have progressively increased since the first commercial 3D instruments were introduced in the 1980s.[2] One of the opportunities provided by 3D printing in health care is to move toward the grand vision of personalized medicine, where treatments are tailored to individual needs rather than the broad patient population.[3] Personalized medicine has been mainly developed to address the inherent limitations of systemic, generalized therapies in health care. 3D printing technology intersects with personalized medicine by creating systems that take individual variabilities into account. In the context of personalized drug delivery systems (DDSs), 3D printing provides invaluable advantages over conventional pharmaceutical manufacturing methods (e.g., molding and compacting) that are based on representative response profiles from associated divisions of the target population. In particular, 3D printing allows for: 1) the manufacture of customized drug tablets and/or drug-eluting implants with precise geometries; 2) flexibility in terms of drug dosages and release profile of medications personalized to the needs of individual patients; and 3) the fabrication of complex drug testing systems that resemble in vivo conditions.

The U.S. Food and Drug Administration's approval of the first 3D-printed drug SPRITAM for epilepsy (marketed by Aprecia Pharmaceuticals in 2015)[4] prompted increasing interest in using 3D printing in personalized medicine.[3] Thus far, 3D printing technology has shown great promise in pharmaceutical manufacturing processes,[5] especially for oral solid dosage,[6,7] transdermal delivery,[8] and drug-eluting implants.[9] Nevertheless, 3D printing in personalized medicine is still in its early stage of development and there are several challenges before mainstream adoption.[5] Aside from regulatory clearance and clinical trials, one of the foremost challenges is the selection of appropriate 3D technologies and formulations suitable for the

A. Bagheri, A. A. Rosser, C. M. Fellows, T. C. Brown
School of Science and Technology
University of New England
Armidale, NSW 2351, Australia
E-mail: ali.bagheri@une.edu.au

M. Asadi-Eydivand
Department of Biomedical Engineering
Amirkabir University of Technology
Tehran 15914, Iran

The ORCID identification number(s) for the author(s) of this article can be found under https://doi.org/10.1002/adem.202201785.

**ADVANCED
SCIENCE NEWS**

www.advancedsciencenews.com

**ADVANCED
ENGINEERING
MATERIALS**

www.aem-journal.com

pharmaceutical product.[10] A particularly versatile and promising 3D printing technology uses photopolymerization in stereolithography (SLA) and digital light processing (DLP).[11,12] These techniques work by decoding a digitally sliced 3D model into physical materials in a layer-by-layer curing process.[13–20] The SLA technology is based on point-by-point exposure as opposed to DLP with the light source illuminating each layer all-at-once. SLA has been used to 3D print oral dosage materials containing 4-aminosalicylic acid and paracetamol,[6] multi-layer oral tablets containing antihypertensive drugs,[21] and ibuprofen-loaded hydrogels.[22] DLP 3D printing has been employed to manufacture oral tablets with different release profiles of theophylline drugs.[23] The impact of resin components on the release profile of paracetamol from DLP-printed tablets has been studied.[24] Moreover, the influence of cure time and wavelength of the photon source (used in a light-based 3D printing) on the release profile of ibuprofen from 3D-printed tablets has been investigated.[25]

Photocuring in light-based 3D printing relies on conventional radical polymerization. Materials produced in this way contain dead polymer chains/strands that cannot be modified after printing. One way to enable post-manufacturing modification is by the application of reversible deactivation radical polymerization (RDRP) to the polymer networks. Dormant RDRP species can be reactivated in a post-synthetic stage to allow the shape, structure, functionality, and/or properties of an already fabricated network to be modified.[26–28] Recently, our group[29–31] and others[32–36] have applied reversible addition fragmentation chain transfer (RAFT) polymerization,[37–44] in light-based 3D printing to realize "living" 3D printing; that is, to manufacture reprocessable 3D materials that could undergo repeatable modifications in a post-printing stage. The development of this technology was inspired by studies of polymeric networks containing dynamic covalent bonds[45,46] and studies of polymeric networks incorporating trithiocarbonate chain transfer agents.[28,47]

The scope of RAFT-mediated 3D printing has been progressively evolving, and different photoreaction mechanisms such as photoiniferter,[29,48] photoinduced electron transfer (PET)-RAFT,[30,36] and cationic RAFT[35,49] have been investigated. Applications of RAFT-based 3D printing in self-healing polymers,[31,50] direct laser writing/surface patterning,[33] surface functionalization,[30,32,48] and polymerization-induced microphase separation[51,52] have been reported. Recently our group reported on RAFT-mediated 3D printing of scaffolds with tailored hierarchical porosities and highly resolved micro- and macroscale features.[53] Building on our previous research,[53] we hypothesized that the interconnected channel-pore architecture of 3D-printed scaffolds may allow for a uniform flow distribution of release media inside the scaffolds for the controlled drug release process. Additionally, different pore sizes, porosity percentages, and surface areas may further enable customization of drug release profile and duration. To the best of our knowledge, there is no report on RAFT-mediated 3D printing of customized DDSs with controlled interconnected channel-pore architecture.

Herein, we report on the 3D printing of on-demand DDSs with precise architecture, geometry, and size, and with customizable drug dosage and release profiles based on a range of 3D models and using a commercially available DLP 3D printer. The first step of the process was generating 3D computer-aided design (CAD) models with a variety of structures and porosities. These models were then exploited to 3D print drug-containing materials using poly(ethylene glycol) diacrylate (PEGDA)-based resin formulations. The inclusion of RAFT (as an alternative to commonly used light-absorbing dyes) in the formulations enabled the 3D printing of materials with highly resolved features throughout the continuous architecture, which is not achievable using conventional radical polymerization. Moreover, the impact of the PEGDA molecular weight on the paracetamol release from the 3D-printed scaffolds was studied. The procedure is technically simple and relatively inexpensive. This research represents a significant advancement over our earlier work,[53] in which we showed that 3D printing using RAFT could produce polymers with customized hierarchical porosities. This study demonstrates that RAFT-mediated 3D printing provides additional and complementary possibilities to move toward personalized medicine by producing customizable DDSs that can be used as drug-eluting implants.

2. Results and Discussion

2.1. 3D Printing Drug-Eluting Materials using Conventional Radical Polymerization and RAFT-Mediated Polymerization

Resin formulations containing the following components were prepared: diphenyl (2,4,6-trimethylbenzoyl) phosphine oxide (TPO) as a photoinitiator, poly(ethylene glycol) diacrylate (PEGDA250, average $M_n = 250\,\text{g mol}^{-1}$) as a crosslinker,[47] poly(ethylene glycol) (PEG300, average $M_n = 300\,\text{g mol}^{-1}$) as a plasticizer/solubilizing agent and paracetamol as a model drug (**Figure 1**, see Supporting Information for methods). TPO enables relatively fast 3D photopolymerization when fully open to air.[54,55] PEGDA is nontoxic, and biodegradable and it has been widely used in materials suitable for tissue and drug delivery applications.[39,56,57] Paracetamol has been chosen as the drug molecule, while PEG is an FDA-approved component commonly used in biomaterials.

Paracetamol absorbs ultraviolet (UV) light with maximum absorbance (λ_{max}) at 243 nm. TPO exhibits strong absorbance in the UV from 300 to 400 nm ($\lambda_{\text{max}} = 380$ nm) and weak absorbance from 400 to 420 nm. To avoid absorbance overlap, the printability of formulations without the presence of paracetamol was initially studied using a commercially available digital light processing (DLP) 3D printer with 405 nm LED lights (1.8 mW cm^{-2}). A series of formulations with different feed ratios were prepared and the 3D printing parameters were adjusted using slicing software. In the first optimization step, a CAD model of a full cylinder (1 cm diameter and 5 mm thick) was used (Figure S1, Supporting Information,). A formulation of [PEGDA250]: [PEG300]:[TPO] = 1:4:0.01 was used with a cure time of 30 s per 500 μm layer (**Table 1**, entry 1). This system did not allow for the production of a well-defined structure, which was attributed to the low amount of crosslinkers relative to the filling agent. The structures of the layer-by-layer 3D-printed objects were confirmed by both optical and scanning electron microscopy (SEM) and considered well-defined as specified in our previous study.[53] We then kept the same
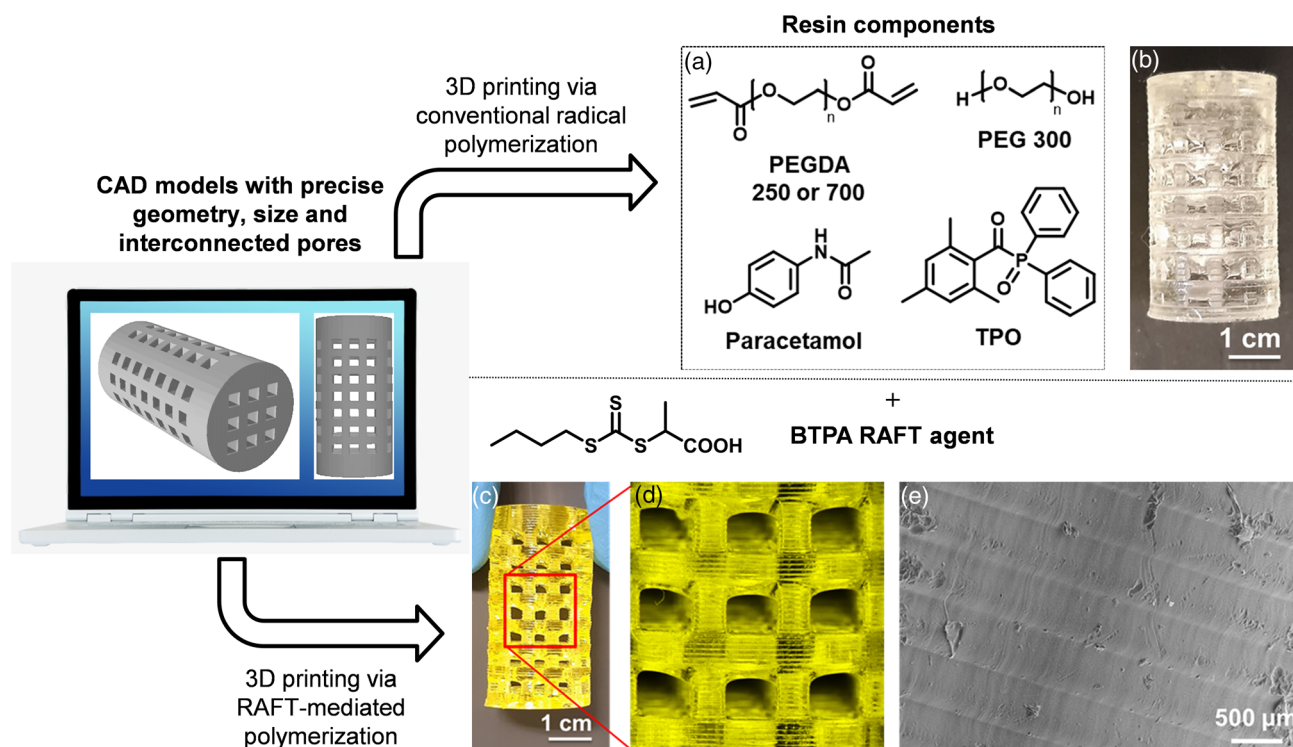
**ADVANCED
SCIENCE NEWS**

www.advancedsciencenews.com

**ADVANCED
ENGINEERING
MATERIALS**

www.aem-journal.com

Figure 1. 3D design and 3D printing approaches used in this study; a) Chemical structures of the resin formulation components used in this work: poly(ethylene glycol) diacrylate (PEGDA250, $M_n = 250$ g mol^{-1} or PEGDA700, $M_n = 700$ g mol^{-1}), polyethylene glycol (PEG300, $M_n = 300$ g mol^{-1}), diphenyl (2,4,6-trimethylbenzoyl) phosphine oxide (TPO), 2-(butylthiocarbonothioylthio) propanoic acid (BTPA), and paracetamol was used as a drug; b) optical image of a 3D-printed scaffold using conventional radical polymerization; c) optical image of a 3D-printed scaffold using RAFT-mediated polymerization in presence of BTPA; d) a representative microscopic image of the scaffold taken using a Nikon SMZ25 stereo microscope which was equipped with DS-Ri1 color-cooled digital camera; e) representative SEM image of a RAFT-based 3D-printed cylinder with 500 μm layer thickness.

printing parameters, while a resin formulation with higher content of PEGDA250 crosslinker was used ([PEGDA250]:[PEG300]:[TPO] = 1:2:0.01). Under these conditions, overcuring around the object was observed (Table 1, entry 2), which could be avoided by reducing exposure time. It was found that 3D printing of a formulation of [PEGDA250]:[PEG300]:[TPO] = 1:2:0.01 with a cure time of 12 s per 500 μm layer allowed the 3D printing of well-defined objects (Table 1, entry 3).

Having determined the formulations and conditions for the manufacture of well-defined objects in the commercial DLP 3D printer, the next step was to include paracetamol. When 2% w/w of paracetamol is added to the formulation, the cure time needed to be extended from 12 to 50 s per 500 μm layer to achieve a well-defined 3D-printed construct (Table 1, entry 9). This increase in cure time was attributed to the light absorbance of paracetamol in the UV range (Figure S2, Supporting Information), competing with the TPO photoinitiator in light absorbance, resulting in a lower rate of radical generation and thus a lower rate of photopolymerization/curing.

Inspired by scaffolds exploited in drug delivery systems,[58,59] cylindrical scaffolds with tailored hierarchical porosities and interconnected morphologies were engineered using 3D design software, SolidWorks 2012, and exported as STL (Standard Triangle Language) files (Figure 1). These CAD models were then employed for 3D printing using [PEGDA250]:[PEG300]:[TPO] = 1:2:0.01% and 2% w/w of paracetamol with a cure time of 50 s per 500 μm layer. Under these conditions, polymerized mass formed within the pores, producing materials with poor resolution (Table 1, entry 10 and Figure 1b). To enhance the Z-axis resolution, 3D printing of thinner layers with shorter cure times was attempted (400 μm and 40 s; 100 μm layer and 25 s (Table 1, entry 11 and 14). Under these conditions, 3D-printed samples also showed polymerized mass within the pores. While adjusting the 3D printing parameters to 25 s cure time per 100 μm layer resulted in materials with better resolution, polymerized mass within the pores was still obvious (Figure S3, Supporting Information).

The occurrence of overcuring in light-based 3D printing systems is mainly due to light scattering and penetration into deeper layers.[1] Limiting overcuring is always a challenge, especially in the process of manufacturing highly porous materials with small internal features. Typically, light-absorbing dyes and radical quenchers are added to the resin formulations to prevent light scattering/penetration and therefore lessening the overcuring.[59] These dyes normally give intense coloring to the printed materials, which can be undesirable. More critically, for materials that are designed for in vivo applications, the release of dyes that are not covalently bonded to the polymer network is highly possible, leading to undesirable reactions/side effects.

Table 1. Details of 3D printing via conventional radical polymerization and RAFT-mediated polymerization using a commercial DLP 3D printer with 405 nm led lights (1.8 mw cm^{-2}).

Entry	[PEGDA250]:[PEG300]:[TPO]	Drug [2% w/w]	3D CADmodel	Target layer thickness [μm][a]	Exposure timeper layer [s][a]	Well definedobject?[b]
1	1:4:0.02	–	Full cylinder	500	30	No
2	1:2:0.01	–	Full cylinder	500	15	No (overcured)
3	1:2:0.01	–	Full cylinder	500	12	Yes
4	1:2:0.01	–	Full cylinder	500	8	No
5	1:2:0.01	Paracetamol	Full cylinder	500	12	No
6	1:2:0.01	Paracetamol	Full cylinder	500	20	No
7	1:2:0.01	Paracetamol	Full cylinder	500	30	No
8	1:2:0.01	Paracetamol	Full cylinder	500	40	No
9	1:2:0.01	Paracetamol	Full cylinder	500	50	Yes
10	1:2:0.01	Paracetamol	Porous Cylinder	500	50	Yes/No[c]
11	1:2:0.01	Paracetamol	Porous Cylinder	400	40	Yes/No[c]
12	1:2:0.01	Paracetamol	Porous Cylinder	100	15	No
13	1:2:0.01	Paracetamol	Porous Cylinder	100	20	No
14	1:2:0.01	Paracetamol	Porous Cylinder	100	25	Yes/No[c]
	[PEGDA250]:[PEG300]:[BTPA]:[TPO]					
15	1:2:0.01:0.01	Paracetamol	Porous Cylinder	500	50	Yes
16	1:2:0.01:0.01	Paracetamol	Porous Cylinder	400	40	Yes
17	1:2:0.01:0.01	Paracetamol	Porous Cylinder	100	25	Yes

[a]Parameters are adjusted by slicing software; [b]A 3D-printed material was considered well-defined from microscope analysis if: i) the layer thicknesses were consistent as defined in the slicing software, ii) the pore sizes, features, and edges of the printed objects were consistent with the CAD models, iii) the material adhered to the build platform throughout the whole 3D printing process, and iv) no significant overcuring around the object or within the pores was observed; [c]3D printing was successful, however, polymerized mass formed within the pores (Figure S3, Supporting Information). All 3D printings were conducted under ambient conditions and without deoxygenation. CAD models of porous cylinders are in Table 2.

Our group[53] and others[34] have recently reported that RAFT-mediated polymerization as opposed to conventional radical polymerization can significantly improve the resolution of the 3D-printed materials by preventing overcuring of the polymers within both the build layer and deeper layers. RAFT agents can act as both photoabsorbers and chain transfer agents. Through light absorption, light scattering can be reduced, and confining curing to exposure precincts. Moreover, the control of molar mass by RAFT agents may result in more controlled photopolymerization within the build layer.[34] Note that RAFT-mediated 3D printing offers additional possibilities that are not achievable using conventional manufacturing techniques. In particular, RAFT enables the production of 3D materials with "living" character, making post-printing modification/patterning possible through reactivation of the dormant network-bound RAFT species.[26] Once the final product is fully formed, RAFT end-groups can be also readily removed or transformed into benign/bioactive functionalities.[60]
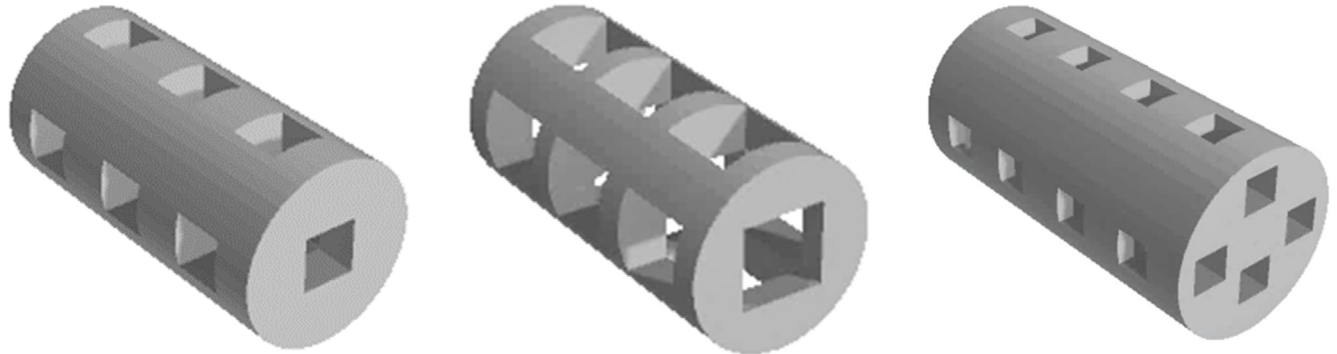
To investigate the possibility of enhanced resolution with RAFT polymerization, a commonly used RAFT agent, 2-(butylthiocarbonothioylthio) propanoic acid (BTPA) was added to the resin formulation using a molar ratio of [PEGDA250]:[PEG300]:[BTPA]:[TPO]=1:2:0.01:0.01 containing 2% w/w of paracetamol (Figure 1). TPO photoinitiator enables relatively fast oxygen-tolerant RAFT-mediated 3D photopolymerization via a "polymerization through" mechanism.[54,55] That is, a portion of generated radicals (through homolytic cleavage of TPO under light exposure) consumes dissolved oxygen through conversion to inert peroxy radicals, allowing propagating radicals to undergo RAFT processes. A CAD model of a porous cylinder with 45% porosity was designed and 3D-printed with 40 mm height and 20 mm diameter, while 3D parameters were set at 50 s cure time per 500 μm layer (Table 1, entry 15). Optical microscopy and SEM were used to demonstrate the resolution of scaffolds printed using RAFT-based formulations. Optical microscope images show that the 3D-printed scaffolds have well-defined geometries as per CAD models with μm resolution throughout the continuous structure and within the pores (Figure 1c,d). SEM images show that the 3D-printed scaffolds have highly resolved micro- and macroscale features, with high accuracy in layer uniformity and thickness as predefined using slicing software (Figure 1e). 3D printing of thinner layers with shorter cure times was also successful (400 μm and 40 s; 100 μm layer and 25 s (Table 1, entry 16 and 17). Under similar conditions, cylindrical scaffolds (**Table 2**) with 65% porosity (pore size of 4.5 mm) and 31% porosity (pore size of 2 mm) were successfully 3D-printed with well-defined features as shown in **Figure 2**. These experiments confirm that RAFT-mediated photopolymerization allows for the manufacture of drug-eluting systems with precise shape, size, and features.

Having determined the 3D printing conditions and resin formulations that allow successful 3D printing, the next step was

Table 2. Specifications of the CAD 3D models for cylindrical scaffolds (angled view) with 20 mm height and 10 mm diameter.

i) Pore size: 3 mm	ii) Pore size: 4.5 mm	iii) Pore size: 2 mm
Porosity: 35%	Porosity: 65%	Porosity: 31%
Pore volume[a]: 549.5 mm^3	Pore volume[a]: 1021 mm^3	Pore volume[a]: 486.7 mm^3
Surface area: 1271.6 mm^2	Surface area: 1129.6 mm^2	Surface area: 1480.4 mm^2

[a]Pore volume = net volume of a full cylinder × porosity percentage. The values presented in this table are based on a full cylinder with a volume of 1570.8 mm^3.
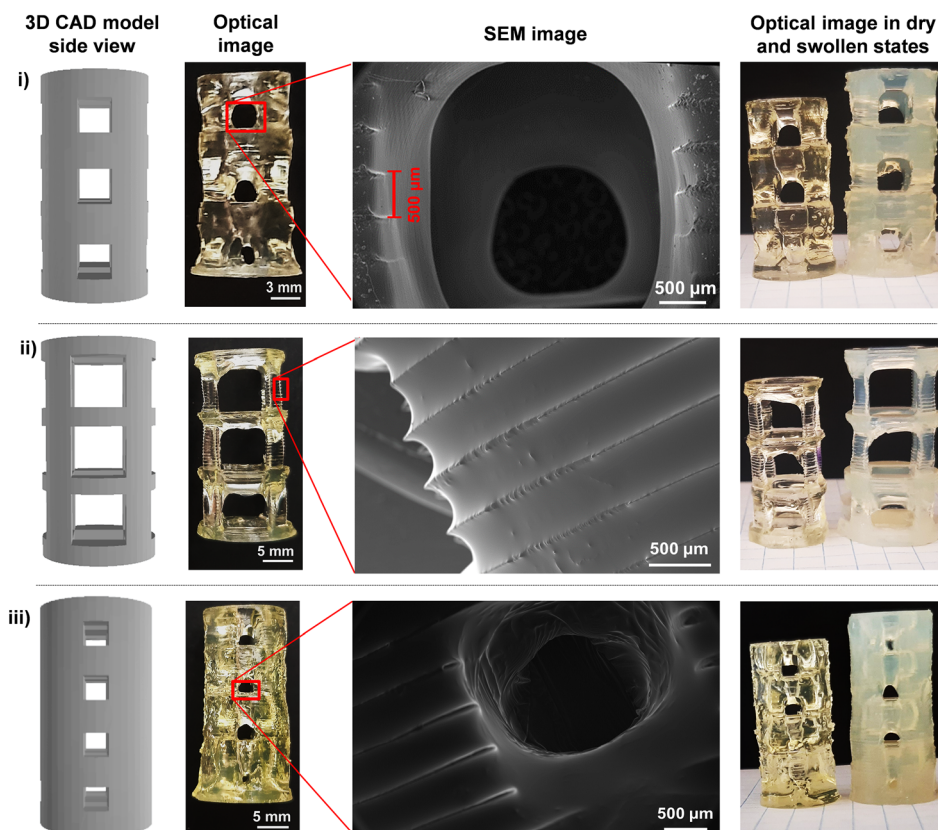

Figure 2. Characterization of the porous cylinders 3D printed using a bottom-up digital light processing (DLP) printer equipped with 405 nm LED lights, at room temperature and fully open to air. (Left) Side views of computer-aided design (CAD) models (refer to Table 2 for specifications), (Middle) optical images and representative SEM images of the 3D-printed scaffolds with 500 μm layer thickness showing the pores and struts of the scaffolds as per the original CAD designs. Scaffold i) was 3D printed with 20 mm height and 10 mm diameter, and scaffolds ii and iii) were 3D printed with 30 mm height and 15 mm diameter; (Right) optical images of 3D scaffolds in a fully swollen state in PBS (original images of the scaffolds are also presented for the sake of comparison—these samples were all 3D printed with 30 mm height and 15 mm diameter). Resin formulation of [PEGDA700]:[PEG300]:[BTPA]:[TPO] = 1:2:0.01:0.01% and 2%, w/w of paracetamol was used in all samples.

**ADVANCED
SCIENCE NEWS**

www.advancedsciencenews.com

**ADVANCED
ENGINEERING
MATERIALS**

www.aem-journal.com

to study the in vitro drug release from the fabricated materials. The in vitro paracetamol release was done in triplicate and a phosphate-buffered saline (PBS, pH 7.4 ± 0.2) was used as the release media. The concentration of released paracetamol in the release media at different time intervals was analyzed using UV–vis spectroscopy at 243 nm (see Supporting Information for details).[24] Paracetamol release from all materials fabricated using PEGDA 250 showed less than 15% release over 90 days. The slow and limited release rate can be attributed to tightly cross-linked networks formed using PEGDA 250, which limits solvent ingression, and thus swelling capacity, resulting in limited drug release. To confirm that the limited release rate was mainly due to high crosslinking density and not insufficient solubility, we conducted control experiments using a model compound. A resin formulation of [PEGDA250]:[PEG300]:[TPO] = 1:2:0.01 containing 0.1% w/w of Nile red was prepared and 3D printed. Nile red was selected as a model drug for ease of quantification as it absorbs light in the visible region. The release of Nile red in dimethyl sulfoxide (DMSO) as a release media was monitored using UV–vis spectroscopy over a 90-day period. Regardless of the CAD model used, the release amount remained below 10%.

2.2. 3D printing Drug-Eluting Materials using PEGDA700 as a Crosslinker (PEGDA700 versus PEGDA250)

We then reasoned that increasing the number of ethylene glycol units between acrylate terminal groups of the crosslinker could increase the small molecule drug release from the 3D-printed materials due to decreased crosslink density, increased system swelling, and increased polymer-water interaction. To test this, PEGDA250 (average units of ethylene oxide = 3) was replaced with PEGDA700 (average units of ethylene oxide = 14), while the other components of the resin formulations were unchanged. PEGDA700 is a crosslinker frequently utilized in light-based 3D printing systems, notably in pharmaceutical and bio-related investigations since it is non-toxic and biocompatible.[61–63] It should be noted that polymers having a terminal RAFT moiety have been extensively studied for their toxicity and have been found to be both easy to remove after manufacture and nontoxic in vitro.[64]

Changes to the crosslinker average molecular weight can affect printability, so 3D printing parameters were varied to optimize the printing. Initially, parameters as per entry 17 in Table 1 were used: Cure time of 25 s per 100 μm layer and PEGDA250 was replaced with PEGDA700; all other parameters were kept constant. This system did not allow for the production of a well-defined object, which can be attributed to the low crosslinking density that was not sufficient to set the layers. Increasing the cure time to 50 s and target thickness to 500 μm enabled 3D printing of well-defined materials using PEGDA700 across all CAD models, indicating that poor printability caused by reduced crosslinking density can be counteracted by a higher cure time.

For a full cylinder, 3D printed using [PEGDA700]:[PEG300]:[BTPA]:[TPO = 1:2:0.01:0.01 containing 2% w/w of paracetamol, the swelling ratio value is found to be between 1.51 and 1.68 in PBS. The swelling ratio is defined as W_w/W_d, where W_w is the weight of a sample swollen in a specified solvent

at room temperature and W_d is the weight of the sample in the dry state. These samples remained as an intact network with no breakage of the matrix in a fully swollen state in PBS. In contrast, the swelling ratio of full cylinders 3D printed using PEGDA250 remained below 1.05% in PBS, and most of the PEGDA250 samples showed breakage of the matrix and different degrees of disintegration into fragments in water. We then attempted to determine the swelling capacity of highly porous scaffolds 3D printed using CAD models in Table 2. The swelling ratios were found to be 1.32 for structure i), 1.33 for structure ii), and 1.29 for structure iii). Overall, PEGDA 700 porous scaffolds were stable and remained as an intact network in fully swollen states (in PBS) across all samples (Figure 2).

Having demonstrated that greater spacing between crosslinking points facilitates greater swelling and so diffusion of water within the crosslinked materials, the next step was to study the release of paracetamol from 3D-printed materials fabricated using PEGDA700 via the RAFT-mediated process. Three CAD cylindrical models with distinct interconnected hierarchical porosities and pore sizes were designed using SolidWorks 2012 and exported as STL files (specifications are listed in Table 2) The interconnected channel-pore architecture was designed to enable a homogeneous flow distribution of release media inside the scaffolds during the drug release process. Additionally, to enable customization of the drug release profiles and duration from 3D materials, models with different pore sizes, porosity percentages, and surface areas were designed (Table 2). The 3D CAD models were sliced digitally with 500 μm layer/slice thickness (and 50 s cure time per layer) and then used in a DLP 3D printing with [PEGDA700]:[PEG300]:[BTPA]:[TPO] = 1:2:0.01:0.01% and 2%, w/w of paracetamol.

The morphology of the 3D-printed materials was studied using a Nikon SMZ25 stereo microscope. Optical images confirmed a precise construction of the original CAD models with outstanding control over both the exterior and interior features. As shown in Figure 2, optical images show distinct 500 μm layers from a cross-sectional view of the RAFT-driven 3D-printed porous scaffolds. SEM images were also recorded, showing fine features around the pores and throughout the continuous structure with μm resolution (Figure 2). Such a high degree of control in fabricating porous materials is not possible using conventional manufacturing techniques such as solvent casting, gas foaming freeze-drying, thermally induced phase separation, and gas foaming.[65,66]

To study in vitro paracetamol release, the PEGDA700 3D-printed scaffolds were placed in a glass media bottle containing 50 mL PBS (pH 7.4 ± 0.2), and then incubated at $37 \pm 0.5\,°C$ and 25 RPM with each sample analyzed in triplicate. The concentration of released paracetamol in the release media was analyzed using UV–vis spectroscopy at 243 nm. The results in **Figure 3**a show that initially the release rate of the drug increases rapidly and within the first 12 h of incubation in PBS a maximum release of paracetamol is reached at more than 50%. Release rates over a 2 week period show further fluctuating increases in Figure 3b, and maximum release was between 60% and 75% from all the porous samples 3D printed with [PEGDA700]:[PEG300]:[BTPA]:[TPO] = 1:2:0.01:0.01% and 2%, w/w of paracetamol. As predicted, drug release profiles differed based on the 3D designs. We postulated that larger pore sizes would result in
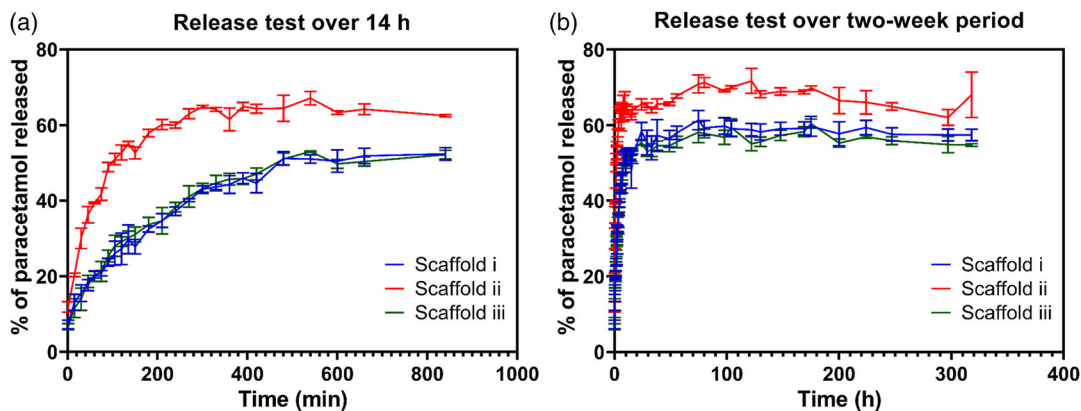
**ADVANCED
SCIENCE NEWS**

www.advancedsciencenews.com

**ADVANCED
ENGINEERING
MATERIALS**

www.aem-journal.com

Figure 3. Percentage cumulative release of paracetamol from 3D-printed scaffolds over: a) first 14 h and b) 2 week period. Cylindrical scaffolds with 30 mm height and 20 mm diameter were 3D printed based on the CAD models listed in Table 2. Resin formulation of [PEGDA700]:[PEG300]:[BTPA]:[TPO] = 1:2:0.01:0.01% and 2%, w/w of paracetamol was used in all samples.

higher water ingression into the system when infiltrated by an aqueous release medium, thus causing higher release rates. This hypothesis was reflected in the paracetamol release results, with structure ii) (Table 2) with 4.5 mm pore sizes showing a higher release rate compared to structure i) with 3 mm pore sizes and structure iii) with 2 mm pore sizes. We also postulated that
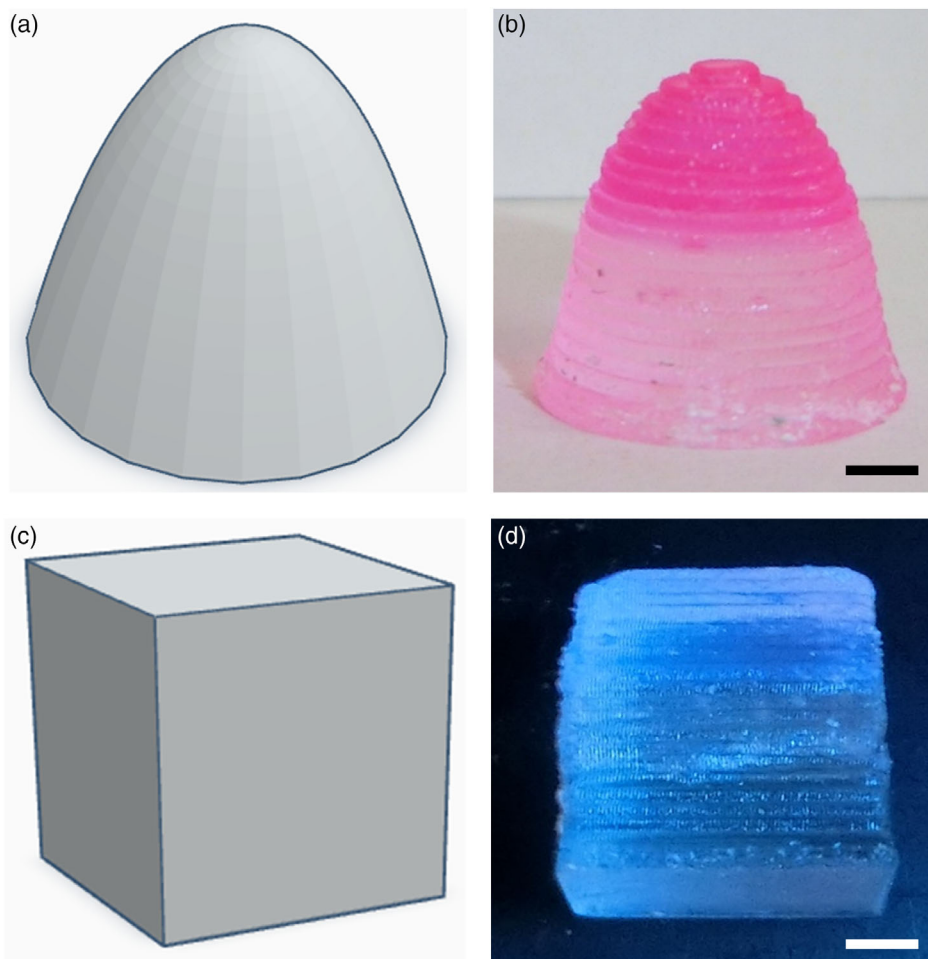

Figure 4. a) CAD model and b) optical image of a 3D-printed structure showing spatiotemporal control in Nile red loading and compositions in different layers; c) CAD model and d) optical image (under 365 nm UV light). of a 3D-printed structure with PyMA loaded in different layers throughout the 3D printing process. Scale bar = 2 mm.

2201785 (7 of 9)

structures with less porosity would show a lower release rate. Structure i) with 35% porosity and structure iii) with 31% porosity clearly show lower release rates than structure ii) with 65% porosity (Figure 3). These findings reveal that the release profile is dependent on system porosity, pore size, and surface area and this approach has the capability to control drug release by optimizing the design of the interconnected channel-pore structure and geometric proportions. That is, 3D-printed DDS can be tailored by carefully adjusting the geometry and porosity of the systems depending on the needs of the patient. We are now conducting systematic experiments in our laboratory to determine how 3D architectures with different features affect the release profile of medications.

To further investigate the applicability of our system in personalized medicine, we demonstrated proof-of-concept examples of 3D-printed drug-eluting scaffolds with more than one drug, spatially separated and incorporated into the same system. Traditionally, medications are administered via separate dosage forms, which is inconvenient and may result in errors and reduced patient compliance. Preferably, multiple medications (customized for every individual) are incorporated in a single dosage form. To demonstrate this, we used a visually distinct dye, Nile red, as the model drug and 3D-printed materials containing spatially-separated layers with different content of Nile red. This was achieved through a multi-resin vat, where different formulations containing different amounts of Nile red were used in specified layers. A cone (10 mm diameter and 10 mm height) CAD model comprising 20 layers each of depth 500 μm was used in this process, showing spatial separation of the Nile red (**Figure** 4b). Separation was also demonstrated using a fluorescent 1-pyrenemethyl methacrylate (PyMA) monomer. A series of resin formulations with gradient of PyMA monomer concentrations were prepared and used in different layers throughout the 3D printing process. After 3D printing, the sample was thoroughly washed and subjected to a 365 nm UV light, showing a gradient of excimer emission of pyrene units increasing from bottom to top (Figure 4d). These examples demonstrate that drug loading and compositions in drug delivery systems can be spatiotemporally controlled, a feature that is not achievable with conventional pharmaceutical techniques.

3. Conclusion

In this study, we have demonstrated that personalized DDSs with precise geometry, size, drug dosage, and release duration/profiles can be 3D-printed using a range of 3D models designed with specific geometry and porosity. Importantly, RAFT-mediated systems as opposed to conventional radical polymerization enabled 3D printing of DDSs with highly resolved features throughout the continuous macroscale architecture. We have demonstrated that the crosslinking density, swelling capacity, and therefore the drug release profile/rate are significantly influenced by the amount of PEG units between the acrylate functional groups of the crosslinkers. Moreover, this approach allowed spatiotemporal control of the drug loading and compositions within different layers of the 3D-printed scaffolds. Our approach is relatively simple and inexpensive to implement. This methodology has the potential to produce personalized DDSs in a clinical setting, using a commercially available 3D printer, immediately following prescription. We believe that these results present an important step towards achieving the aim of personalized medicine. In addition to delivering medications, this technique can be exploited to deliver other active substances with desired release profiles, and so may have implications in foods, cosmetics, and the agricultural industries. Future work will focus on the effect of pore size, porosity, and surface area of the 3D-printed scaffolds on the release profile of medications.

Conflict of Interest

The authors declare no conflict of interest.

Data Availability Statement

The data that support the findings of this study are available in the supplementary material of this article.

[1] A. Bagheri, J. Jin, *ACS Appl. Polym. Mater.* **2019**, *1*, 593.

[2] S. C. Ligon, R. Liska, J. Stampfl, M. Gurr, R. Mülhaupt, *Chem. Rev.* **2017**, *117*, 10212.

[3] F. S. Collins, H. Varmus, *N. Engl. J. Med.* **2015**, *372*, 793.

[4] C. C. Carey, *Clinical Engineering Handbook*, 2nd ed., Mara Conner, USA **2019**, pp. 764–773.

[5] S. H. Lim, H. Kathuria, J. J. Y. Tan, L. Kang, *Adv. Drug Delivery Rev.* **2018**, *132*, 139.

[6] J. Wang, A. Goyanes, S. Gaisford, A. W. Basit, *Int. J. Pharm.* **2016**, *503*, 207.

[7] I. Karakurt, A. Aydoğdu, S. Çıkrıkcı, J. Orozco, L. Lin, *Int. J. Pharm.* **2020**, *584*, 119428.

[8] A. Goyanes, U. Det-Amornrat, J. Wang, A. W. Basit, S. Gaisford, *J. Controlled Release* **2016**, *234*, 41.

[9] B. Zhang, S. Li, H. Hingorani, A. Serjouei, L. Larush, A. A. Pawar, W. H. Goh, A. H. Sakhaei, M. Hashimoto, K. Kowsari, S. Magdassi, Q. Ge, *J. Mater. Chem. B* **2018**, *6*, 3246.

[10] J. Norman, R. D. Madurawe, C. M. V. Moore, M. A. Khan, A. Khairuzzaman, *Adv. Drug Delivery Rev.* **2017**, *108*, 39.

[11] M. Layani, X. Wang, S. Magdassi, *Adv. Mater.* **2018**, *30*, 1.

[12] J. Zhang, P. Xiao, *Polym. Chem.* **2018**, *9*, 1530.

[13] J. Lee, H. C. Kim, J. W. Choi, I. H. Lee, *Int. J. Precis. Eng. Manuf. Green Technol.* **2017**, *4*, 373.

[14] A. Sydney Gladman, E. A. Matsumoto, R. G. Nuzzo, L. Mahadevan, J. A. Lewis, *Nat. Mater.* **2016**, *15*, 413.

[15] F. Momeni, S. M. Mehdi Hassani.N, X. Liu, J. Ni, *Mater. Des.* **2017**, *122*, 42.

[16] H. Yang, W. R. Leow, T. Wang, J. Wang, J. Yu, K. He, D. Qi, C. Wan, X. Chen, *Adv. Mater.* **2017**, *29*, 1701627.

[17] S. Dutta, D. Cohn, *J. Mater. Chem. B* **2017**, *5*, 9514.

[18] I. Roppolo, A. Chiappone, A. Angelini, S. Stassi, F. Frascella, C. F. Pirri, C. Ricciardi, E. Descrovi, *Mater. Horiz.* **2017**, *4*, 396.

[19] Z. Zhao, X. Kuang, C. Yuan, H. J. Qi, D. Fang, *ACS Appl. Mater. Interfaces* **2018**, *10*, 19932.

[20] M. Gernhardt, E. Blasco, M. Hippler, J. Blinco, M. Bastmeyer, M. Wegener, H. Frisch, C. Barner-Kowollik, *Adv. Mater.* **2019**, *31*, 1.

[21] X. Xu, P. Robles-Martinez, C. M. Madla, F. Joubert, A. Goyanes, A. W. Basit, S. Gaisford, *Addit. Manuf.* **2020**, *33*, 101071.

[22] P. R. Martinez, A. Goyanes, A. W. Basit, S. Gaisford, *Int. J. Pharm.* **2017**, *532*, 313.

[23] H. Kadry, S. Wadnap, C. Xu, F. Ahsan, *Eur. J. Pharm. Sci.* **2019**, *135*, 60.

[24] M. Krkobabić, D. Medarević, S. Cvijić, B. Grujić, S. Ibrić, *Int. J. Pharm.* **2019**, *572*, 118790.

[25] M. Madžarević, S. Ibrić, *Eur. J. Pharm. Sci.* **2021**, *158*, 105688.

[26] A. Bagheri, C. M. Fellows, C. Boyer, *Adv. Sci.* **2021**, *8*, 2003701.

[27] J. Cuthbert, A. C. Balazs, T. Kowalewski, K. Matyjaszewski, *Trends Chem* **2020**, *2*, 341.

[28] M. Chen, Y. Gu, A. Singh, M. Zhong, A. M. Jordan, S. Biswas, L. T. J. Korley, A. C. Balazs, J. A. Johnson, *ACS Cent. Sci.* **2017**, *3*, 124.

[29] A. Bagheri, K. E. Engel, C. W. A. Bainbridge, J. Xu, C. Boyer, J. Jin, *Polym. Chem.* **2020**, *11*, 641.

[30] A. Bagheri, C. W. A. Bainbridge, K. E. Engel, G. G. Qiao, J. Xu, C. Boyer, J. Jin, *ACS Appl. Polym. Mater.* **2020**, *2*, 782.

[31] A. Bagheri, H. Ling, C. W. A. Bainbridge, J. Jin, *ACS Appl. Polym. Mater.* **2021**, *3*, 2921.

[32] Z. Zhang, N. Corrigan, A. Bagheri, J. Jin, C. Boyer, *Angew. Chem.* **2019**, *58*, 17954.

[33] X. Wu, B. Gross, B. Leuschel, K. Mougin, S. Dominici, S. Gree, M. Belqat, V. Tkachenko, B. Cabannes-Boué, A. Chemtob, J. Poly, A. Spangenberg, *Adv. Funct. Mater.* **2021**, *32*, 2109446.

[34] K. Lee, N. Corrigan, C. Boyer, *Angew. Chem.* **2021**, *60*, 8839.

[35] B. Zhao, J. Li, X. Pan, Z. Zhang, G. Jin, J. Zhu, *ACS Macro. Lett.* **2021**, *10*, 1315.

[36] X. Shi, J. Zhang, N. Corrigan, C. Boyer, *Polym. Chem.* **2022**, *13*, 44.

[37] G. Moad, *Polym. Int.* **2015**, *64*, 15.

[38] G. Moad, E. Rizzardo, S. H. Thang, *Aust. J. Chem.* **2002**, *58*, 379.

[39] M. R. Hill, R. N. Carmean, B. S. Sumerlin, *Macromolecules* **2015**, *48*, 5459.

[40] T. G. McKenzie, Q. Fu, M. Uchiyama, K. Satoh, J. Xu, C. Boyer, M. Kamigaito, G. G. Qiao, *Adv. Sci.* **2016**, *3*, 1.

[41] N. Corrigan, K. Jung, G. Moad, C. J. Hawker, K. Matyjaszewski, C. Boyer, *Prog. Polym. Sci.* **2020**, *111*, 101311.

[42] V. Bellotti, R. Simonutti, *Polymers* **2021**, *13*, 1119.

[43] M. Uchiyama, K. Satoh, M. Kamigaito, *Angew. Chem.* **2015**, *127* 1944.

[44] K. Jiang, S. Han, M. Ma, L. Zhang, Y. Zhao, M. Chen, *J. Am. Chem. Soc.* **2020**, *142*, 7108.

[45] C. R. Fenoli, C. N. Bowman, *Polym. Chem.* **2014**, *5*, 62.

[46] H. Y. Park, C. J. Kloxin, M. F. Fordney, C. N. Bowman, *Dent. Mater.* **2012**, *28*, 888.

[47] A. Bagheri, C. Bainbridge, J. Jin, *ACS Appl. Polym. Mater.* **2019**, *1*, 1896.

[48] B. Zhao, J. Li, Y. Xiu, X. Pan, Z. Zhang, J. Zhu, *Macromolecules* **2022**, *55*, 1620.

[49] B. Zhao, J. Li, Z. Li, X. Lin, X. Pan, Z. Zhang, J. Zhu, *Macromolecules* **2022**, *55*, 7181.

[50] Z. Zhang, N. Corrigan, C. Boyer, *Angew. Chem.* **2022**, *61*, e202114111.

[51] T. Maruyama, M. Mukai, R. Sato, M. Iijima, M. Sato, T. Furukawa, S. Maruo, *ACS Appl. Polym. Mater.* **2022**, *4*, 5515.

[52] V. A. Bobrin, Y. Yao, X. Shi, Y. Xiu, J. Zhang, N. Corrigan, C. Boyer, *Nat. Commun.* **2022**, *13*, 1.

[53] M. Asadi-Eydivand, T. C. Brown, A. Bagheri, *ACS Appl. Polym. Mater.* **2022**, *4*, 4940.

[54] L. Lu, N. Yang, Y. Cai, *Chem. Commun.* **2005**, 5287.

[55] L. Lu, H. Zhang, N. Yang, Y. Cai, *Macromolecules* **2006**, *39*, 3770.

[56] M. B. Browning, S. N. Cereceres, P. T. Luong, E. M. Cosgriff-Hernandez, *J. Biomed. Mater. Res. A* **2014**, *102*, 4244.

[57] D. Puppi, F. Chiellini, *Addit. Manuf.* **2020**, *20*, 100700.

[58] M. Asadi-Eydivand, M. Solati-Hashjin, A. Farzad, N. A. Abu Osman, *Robot. Comput. Integr. Manuf.* **2016**, *37*, 57.

[59] D. Ahn, L. M. Stevens, K. Zhou, Z. A. Page, *ACS Cent. Sci.* **2020**, *6*, 1555.

[60] H. Willcock, R. K. O'Reilly, *Polym. Chem.* **2010**, *1*, 149.

[61] A. Chiappone, E. Fantino, I. Roppolo, M. Lorusso, D. Manfredi, P. Fino, C. F. Pirri, F. Calignano, *ACS Appl. Mater. Interfaces* **2016**, *8*, 5627.

[62] N. B. Palaganas, J. D. Mangadlao, A. C. C. De Leon, J. O. Palaganas, K. D. Pangilinan, Y. J. Lee, R. C. Advincula, *ACS Appl. Mater. Interfaces* **2017**, *9*, 34314.

[63] J. Warner, P. Soman, W. Zhu, M. Tom, S. Chen, *ACS Biomater. Sci. Eng.* **2016**, *2*, 1763.

[64] H. Sun, W. Choi, N. Zang, C. Battistella, M. P. Thompson, W. Cao, X. Zhou, C. Forman, N. C. Gianneschi, *Angew. Chem.* **2019**, *131*, 17520.

[65] C. Gao, S. Peng, P. Feng, C. Shuai, *Bone Res.* **2017**, *5*, 1.

[66] N. Karamat-Ullah, Y. Demidov, M. Schramm, D. Grumme, J. Auer, C. Bohr, B. Brachvogel, H. Maleki, *ACS Biomater. Sci. Eng.* **2021**, *7*, 4545.